

# MoE-Enhanced Multi-Domain Feature Selection and Fusion for Fast Map-Free Trajectory Prediction

Wenyi Xiong<sup>1</sup>, Jian Chen<sup>2</sup>, *Senior Member, IEEE*, Ziheng Qi<sup>3</sup>, Wen-hua Chen<sup>4</sup>, *Fellow, IEEE*

**Abstract**—Trajectory prediction is crucial for the reliability and safety of autonomous driving systems, yet it remains a challenging task in complex interactive scenarios due to noisy trajectory observations and intricate agent interactions. Existing methods often struggle to filter redundant scene data for discriminative information extraction, directly impairing trajectory prediction accuracy—especially when handling outliers and dynamic multi-agent interactions. In response to these limitations, we present a novel map-free trajectory prediction method which adaptively eliminates redundant information and selects discriminative features across the temporal, spatial, and frequency domains, thereby enabling precise trajectory prediction in real-world driving environments. First, we design a MoE (Mixture of Experts)-based frequency-domain filter to adaptively weight distinct frequency components of observed trajectory data and suppress outlier-related noise; then a selective spatiotemporal attention module that reallocates weights across temporal nodes (sequential dependencies), temporal trends (evolution patterns), and spatial nodes to extract salient information is proposed. Finally, our multimodal decoder—supervised by joint patch-level and point-level losses—generates reasonable and temporally consistent trajectories, and comprehensive experiments on the large-scale NuScenes and Argoverse dataset demonstrate that our method achieves competitive performance and low-latency inference performance compared with recently proposed methods.

**Index Terms**—Map-free motion prediction, Mixture of Experts mechanism, selective attention.

## I. INTRODUCTION

TRAJECTORY prediction stands as a cornerstone technology in advancing autonomous driving towards full autonomy, as its ability to infer future motion patterns of traffic participants directly underpins the system's capacity for risk anticipation and safe maneuvering, making it a long-standing research hotspot in the field. The introduction of vectorized representation frameworks, typified by VectorNet [1], marked a pivotal shift in trajectory prediction research. Increasingly, modern prediction models leverage vectorized traffic agents (e.g., vehicle trajectories, pedestrian movement paths) and environmental elements to explicitly model interactive relationships within scenes, enabling more targeted

<sup>1</sup>Wenyi Xiong is with the School of Mechanical Engineering, Zhejiang University, Hangzhou 310027, China.

<sup>2</sup>Jian Chen is with the Guangdong Provincial Key Laboratory of Fully Actuated System Control Theory and Technology, School of Automation and Intelligent Manufacturing, Southern University of Science and Technology, Shenzhen 518055, China. He is also with the School of Mechanical Engineering, Zhejiang University, Hangzhou 310058, China. (e-mail: chenj8@sustech.edu.cn).

<sup>3</sup>Ziheng Qi is with Leapmotor Technology, Hangzhou, 310052, China

<sup>4</sup>Wen-hua Chen is with the Department of Aeronautical and Automotive Engineering, Loughborough University, Leicestershire, LE11 3TU, U.K. (email: W.Chen@lboro.ac.uk).

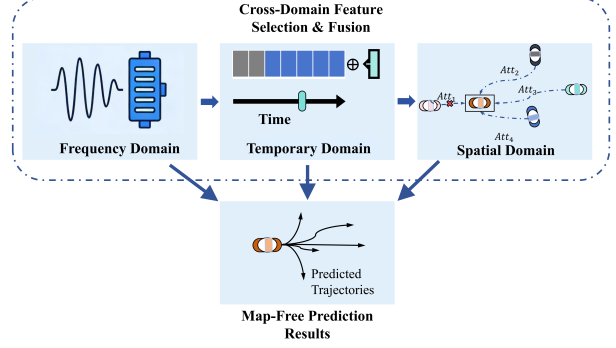


Fig. 1. Schematic of multi-domain feature selection and fusion for map-free trajectory prediction.

capture of critical cues among traffic participants. For instance, graph neural networks (GNNs) [2], [3] have become a staple for relational modeling: models like HDGT [3] construct hypergraphs to encode heterogeneous interactions between the target agent and surrounding entities (e.g., adjacent vehicles, crossing pedestrians), effectively capturing complex multi-agent dependency structures. On the other hand, attention-based methods [4]–[9] such as MTR [10] computes adaptive weights for different interactions relative to the focal agent, dynamically prioritizing impactful environmental elements while aggregating contextual information to refine motion predictions.

Nevertheless, state-of-the-art vectorized models still suffer from two critical unresolved challenges. First, most existing vectorized methods are inherently map-dependent, requiring high-definition (HD) map data for lane topology, road boundaries, and traffic rule constraints [11]. This reliance not only increases data preprocessing computational costs but also severely impairs adaptability—marked performance degradation occurs in unstructured environments or when HD maps are outdated or unavailable. Second, prevalent map-free vectorized methods [12], [13] typically process temporal dynamics and spatial interactions indiscriminately. By incorporating excessive redundant information, these methods fail to distinguish critical motion patterns from irrelevant signals, thus cannot prioritize impactful agent interactions. This flaw induces noisy feature representations, ultimately yielding suboptimal prediction performance.

To address these challenges, we propose a novel map-free trajectory prediction framework that implements redundant noise suppression and important feature selection across the spatial, temporal, and frequency domains (see Fig. 1). Specifi-

cially, to enhance the extraction of discriminative features from historical trajectories, we first integrate a Mixture of Experts (MoE)-driven frequency-domain analysis module [14] to suppress trajectory noise and adaptively prioritize critical frequency components. To fully exploit the intrinsic evolutionary patterns of historical trajectories, we adopt a trend-aware partitioning strategy for historical trajectory information. Building on this, a novel selective attention module is specifically designed to adaptively amplify salient spatiotemporal cues from the extracted temporal node features, temporal trend features, and spatial node features. Finally, deviating from conventional paradigms [11], [12], we introduce a patch-level loss function for prediction supervision. Extensive experiments on the NuScenes and Argoverse datasets demonstrate that our approach achieves competitive performance and low-latency inference performance against state-of-the-art methods.

Based on the above discussion, our contribution is summarized below:

- MoE-driven frequency-domain analysis is integrated to enhance historical feature extraction, enabling adaptive identification of critical frequency components, effective noise suppression, and preservation of trajectory-relevant frequency characteristics.
- A trend-aware partitioning strategy is adopted to decompose historical trajectories. A novel selective attention module is designed to adaptively amplify salient spatiotemporal cues (temporal node, temporal trend, spatial node features) for in-depth mining of trajectory evolutionary patterns.
- A map-free method is proposed to eliminate redundant information and extract key features across multiple domains—freeing from HD map reliance with a novel patch-level loss introduced for prediction supervision, achieving competitive performance on the large-scale NuScenes and Argoverse dataset.

## II. RELATED WORKS AND PROBLEM FORMULATION

### A. Trajectory Prediction Methods

Trajectory prediction enables autonomous driving systems to anticipate future movements in traffic environments, serving as a critical component for ensuring operational safety and decision-making efficiency. In recent years, deep learning has revolutionized trajectory prediction by enabling the extraction of complex data patterns and efficient processing of large-scale datasets. To incorporate environmental constraints, contemporary vehicle trajectory prediction methods have increasingly integrated high-definition (HD) maps in vectorized forms [1]. For example, LaneGCN [2] aggregates interaction features among agent-lane, lane-lane, and agent-agent via adjacency matrices to achieve multimodal trajectory prediction. HDGT [3] models traffic scenarios as heterogeneous graphs of different types to update nodes and edges separately. HiVT [11] extracts interactions from both local and global perspectives, thereby enabling efficient scene modeling. However, the reliance on HD maps—plagued by accessibility issues and high annotation costs—hinders their deployment in complex real-world scenarios. Recognizing these limitations, recent research

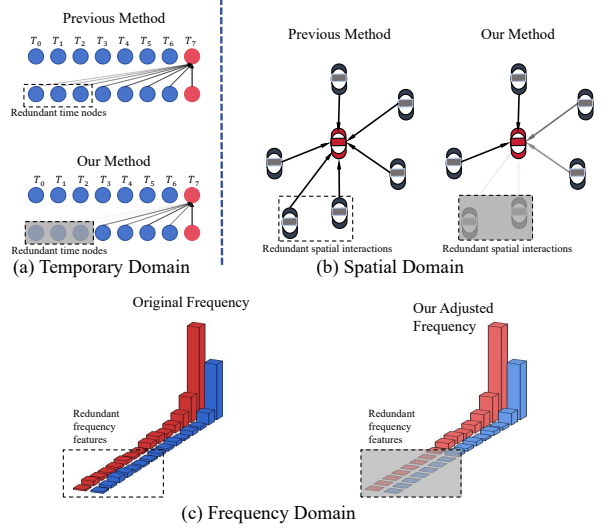


Fig. 2. Comparison of workflows in multiple domains. In the temporal domain, our approach filters out redundant time nodes compared to previous methods. In the spatial domain, we decrease the consideration of redundant interactions. Additionally, we adjust the frequency distribution to suppress some high - frequency noises.

has focused on map-free trajectory prediction [5], [15] as a promising alternative. For instance, MLB [12] models agent-specific modal patterns through local encoding and introduces a trajectory consistency module to mitigate inconsistency issues in map-free prediction. HSTI [13] combines static GCNs with dynamic attention mechanisms to capture multi-agent interactions. Nevertheless, map-free approaches still face critical challenges. Existing map-free vectorized methods [12], [13] incorporate redundant information in handling temporal dynamics, frequency components, and spatial interactions, as depicted in Fig. 2. Previous approaches fail to discriminate critical motion patterns from superfluous signals or prioritize significant agent interactions.

### B. Traffic Multi-domain Feature Modeling

In the realm of temporal modeling, Recurrent Neural Networks (RNNs) [4], [16], [17] rely on hidden states that carry information from previous time steps. However, they suffer from the vanishing gradient problem like recurrent neural units. To address this issue, improved RNN variants such as Long Short-Term Memory (LSTM) [18] and Mamba [12], [19] have emerged. To obtain global features, the Transformer [20] architecture has been introduced [7]. The self-attention mechanism in Transformer allows the model to directly access and weigh all elements in the sequence at once, regardless of their position in the time series. Recently, frequency-domain features have been incorporated to enhance temporal modeling. For instance, the frequencies of trajectories are decomposed to focus on crucial wavelet components, as described in [21], [22]. This approach significantly improves signal modeling by leveraging the properties of the frequency domain. The modeling of spatial features is far more diverse. Vectorsnet's [1] vectorization of scene features has enabled the integration of various modeling methods from other fields

into trajectory prediction. GNN-based algorithms [23] use graphs with nodes representing agents and edges denoting their relationships. Through graph convolutions, information is passed between nodes to model multi-agent interactions for trajectory prediction. Attention-based [11], [12], [24]–[26] algorithms, on the other hand, utilize the attention mechanism to assign weights to spatial elements, enabling the model to focus on relevant features such as agent proximity and motion trends for prediction. Inspired by these approaches, our novel map-free trajectory prediction framework aims to eliminate redundant information and select important spatio-temporal-frequency features as shown in Fig. 2.

### C. Problem Formulation

In a traffic scenario, given the historical observations of all traffic participants, the objective of our task is to predict the future trajectories of target agents. Suppose there are a total of  $N$  agents in the scenario; their historical states are defined as  $\mathbf{X}_h = \{\tau_i^t \mid i \in 1, \dots, N; t \in -T_h + 1, \dots, 0\}$ , where  $\tau_i^t = (x_i^t, y_i^t, v_i^t)$  represents the 2D spatial coordinates and velocity of the  $i$ -th agent at the time step  $t$ , and  $T_h$  represents the length of the historical observation window. Based on this input, the target of our prediction is the future trajectory of target vehicle:  $\mathbf{X}_f = \{\tau_{target}^t \mid t \in 1, \dots, T_f\}$ , where  $T_f$  denotes the future horizon.

## III. PROPOSED MODEL

### A. Cross-Domain Trajectory Prediction Method Overview

Fig. 3 illustrates our cross-domain framework, which jointly processes frequency, temporal, and spatial domain information to eliminate redundant information and prioritize important features. Specifically, unlike prior methods that struggle with redundant temporal nodes, spatial interactions, and high-frequency noise (Fig. 2), a MoE-based frequency domain filter first suppresses noise and distills salient trajectory components. We then adopt a trend-aware temporal selective attention module and a spatial selective attention module to capture critical spatiotemporal cues by filtering irrelevant temporal nodes and spatial interactions. Finally, three losses (point-level, classification, patch-level) supervise the prediction process to ensure accuracy.

### B. MoE-based Frequency-Domain Filter

Unlike prior algorithms [11], [12] that aggregate time nodes without processing, we utilize a Mixture of Experts [14] based frequency filter to reduce the impact of outlier noise. Inspired by [27], a MoE mechanism, enabling adaptive extraction of multiple frequency features is integrated. First, historical trajectories are embedded by simple MLP to get  $\mathbf{E} \in R^{B \times T_h \times C}$ , where  $B$  is the batchsize,  $C$  is the hidden channels. These time-domain trajectory sequences are transformed into the frequency domain using Fourier Transform, yielding complex-valued representations  $\hat{\mathbf{E}}_{h,f}$ . To disentangle frequency-specific features, the frequency spectrum is uniformly partitioned into  $N$  non-overlapping intervals, each assigned to a dedicated expert module. For the  $i$ -th expert, a binary mask is

applied to  $\hat{\mathbf{E}}_{h,f}$ , where  $M_i(b, f, c) = 1$  if the  $b$ -th batch,  $f$ -th frequency falls within the  $i$ -th interval, and 0 otherwise. This masking operation effectively isolates the frequency components relevant to the  $i$ -th expert, resulting in a filtered frequency-domain representation:

$$\hat{E}_{i,h} = M_i \odot \hat{E}_{h,f} \quad (1)$$

where  $\hat{E}_h$  is the masked output. Subsequently, a gating network is introduced to dynamically aggregate the outputs of all individual and specialized experts. Specifically, the gating network takes the original frequency-domain representation  $\hat{\mathbf{E}}_h$  as input:

$$\mathbf{G} = \frac{1}{C} \sum_{c=1}^C |\hat{\mathbf{E}}_h| \quad (2)$$

where  $G$  is the average frequency component. Then, a linear projection is applied to produce the weight scores for each expert:

$$W = \text{SoftMax}(\text{Linear}(G)) \quad (3)$$

where  $W$  is the frequency weight. The weights are utilized to get the final weighted frequency outputs. Finally, the aggregated frequency-domain signal  $\hat{\mathbf{E}}_{out}$  is converted back to the time domain using Inverse Fourier Transform to obtain  $\mathbf{E}_{out}$ .

### C. Trend-aware Temporal-Spatial Domain Selective Attention

1) *Temporal Trend Modeling*: Inspired by [28], we integrate a novel and task-adaptive trend-aware branch to further enhance the capture of dynamic and evolving temporal trend dynamics. As illustrated in Fig. 3, a sliding window with a fixed step size is adopted to extract temporal trends from adjacent time steps, thereby incorporating richer historical information into the network. For each trend, its features are flattened along the time dimension and then projected to the hidden dimension via a Multi-Layer Perceptron (MLP) to generate  $\mathbf{E}_p$ . Notably, such trend embeddings are less sensitive to outlier time nodes, which effectively boosts the model's robustness. Then, the fine-grained  $\hat{\mathbf{E}}_{out}$  and the trend-aware  $\mathbf{E}_p$  are fed into two separate temporal branches to extract features at different scales.

2) *Temporal Selective Attention*: When driving, human drivers usually focus only on certain critical and highly relevant important nodes or trends rather than the entire complex and complete trajectory. However, most current algorithms [11]–[13] fail to take this essential human driving characteristic into account. The consequence of this is that redundant information interferes with the perception of key foreground information, thereby leading to suboptimal prediction performance. To address this issue, we propose a novel selective attention module to suppress redundant components in temporal nodes and temporal trends.

We first assign an different learnable position tokens for trend sequence and point sequence to form  $S_i \in \mathbb{R}^{(P_i+1) \times D_p}$ , where  $P_i$  denotes the length of sequence  $i$  and  $D_p$  denotes the trend hidden size. After that,  $S_i$  are linearly projected to

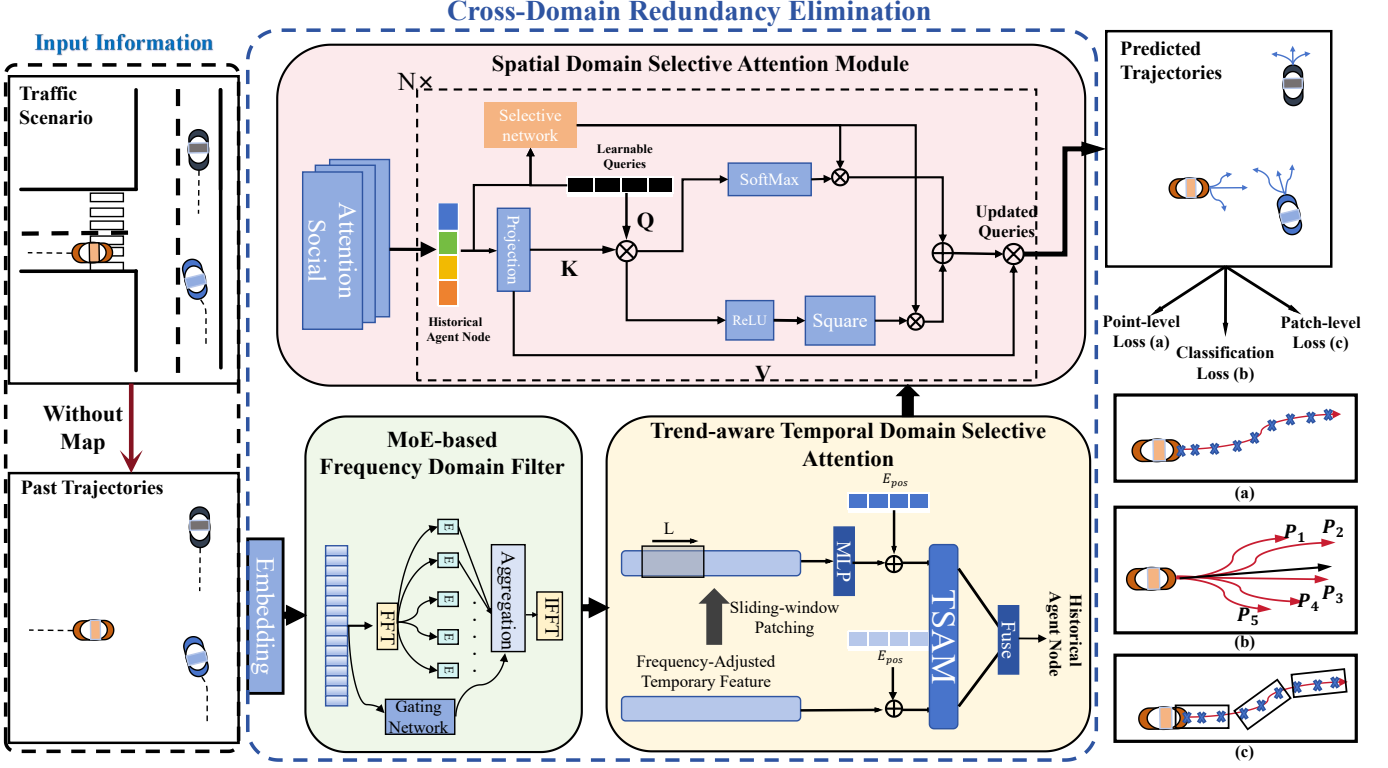


Fig. 3. Overview of the proposed algorithm framework, consisting of three interconnected frequency, time, and space domain components. An MoE-based frequency filter first distills salient components from observed trajectories. Then, a trend-aware temporal selective attention module and a spatial selective attention module capture critical spatiotemporal features. Three losses (point-level, classification, patch-level) supervise the prediction process.

generate query ( $Q_i$ ), key ( $K_i$ ), and value ( $V_i$ ) matrices. The whole temporal selective attention can be written as [29]:

$$A_i = f\left(\frac{Q_i K_i^T}{d_k} + M_i\right) \quad (4)$$

where  $M_i$  denotes the temporal mask enforcing the tokens only considers previous information. Specifically, we compute two types of attention matrices: the standard dense attention matrix that models full pairwise correlations among all agents, and a sparse attention matrix that focuses on semantically meaningful agent pairs:

$$\begin{cases} DA_i = \text{SoftMax}\left(\frac{Q_i K_i^T}{d_k} + M_i\right), \\ SA_i = \text{RELU}^2\left(\frac{Q_i K_i^T}{d_k} + M_i\right) \end{cases} \quad (5)$$

where  $DA_i$  denotes the dense attention scores and  $SA_i$  denotes the sparse attention scores. It can be observed that, through RELU and square operation, the sparse attention (SA) mechanism effectively eliminates negative attention scores and adaptively amplifies the attention weights assigned to critical agents that exert significant impacts on the target's future trajectory. To dynamically weight the outputs of the two attention mechanisms and thus optimize the feature fusion process, we design a novel selective network. The core novelty of this network lies in its pair-wise concatenation strategy, which enables fine-grained feature selection by explicitly modeling the correlation between the inputs of the two attention branches. Specifically, this is achieved by first concatenating their feature

inputs in a pair-wise manner, followed by the computation of an intermediate gate matrix  $R_i \subseteq \mathbb{R}^{(P_i+1) \times (P_i+1) \times 2D_p}$ , where the dimensionality expansion to  $2D_p$  preserves the complete feature information from both branches. Based on this intermediate matrix, a learnable gate matrix is further derived to generated:

$$G_i = \text{Sigmoid}(\text{MLP}(R_i)) \quad (6)$$

where  $G_i$  represent the gate matrix. It acts as a soft selector that dynamically balances the contributions of the two attention mechanisms. The final attention scores are computed as a weighted combination of the two attention outputs:

$$A_i = G_i \cdot DA_i + (1 - G_i) \cdot SA_i. \quad (7)$$

Ultimately, the derived final attention weights are employed to weight the value matrices. We stack multiple temporal selective attention layers for each branch. Finally, the last state from both branches are aggregated through MLPs to get the historical nodes  $E_h$ .

3) *Spatial selective attention module*: Following temporal modeling, we conduct spatial learning on the derived historical node embeddings  $E_h$ . First, stacked social attention layers are deployed to excavate intricate interactive dynamics among heterogeneous agents. Subsequently, we initialize a set of learnable query vectors, where each query is designed to encode a distinct driving mode. These mode-aware queries, along with the historical agent nodes (projected as keys and

values), are fed into a spatial selective attention module, which computes attention weights as follows:

$$A_h = f\left(\frac{Q_h K_h^T}{d_k}\right). \quad (8)$$

Multiple selective attention layers are stacked to iteratively refine the learnable queries. This step is pivotal, as it directly mimics human drivers' instinctive spatial perception mechanism—prioritizing salient agents over irrelevant entities in real-world driving scenarios. Finally, the interaction-aware embeddings  $E_a$  generated through this spatial learning process are fed into the multimodal decoder for subsequent trajectory prediction.

#### D. Patch-level Loss Enhanced trajectory decoder

In this section, trajectory decoder and the loss design is introduced. For generated multimodal  $E_a$ , corresponding MLPs are applied to decode them into future trajectories, velocities and multimodal scores. Similar to the previous approach [10], [11], we calculate their regression loss  $\mathcal{L}_{reg}$  and classification loss  $\mathcal{L}_{cls}$ . Furthermore, inspired by the patch-based modeling paradigm in [30], we innovatively extend this concept to the trajectory prediction domain by introducing a trajectory-adaptive patch-level structural loss, which addresses the limitations of point-level losses in capturing global trajectory consistency. To the best of our knowledge, we are the first to incorporate patch-level structural supervision into multimodal trajectory prediction tasks.

**Patch-level structural loss:** In contrast to most prediction algorithms that solely consider point level loss, the patch level loss takes into account the overall deviation between the prediction and the ground truth. First, akin to the operation in [30], we patchify the predicted trajectory. Patch-level loss are divided into three parts: correlation loss, variance loss, and mean loss.

$$\mathcal{L}_{patch} = \mathcal{L}_{Corr} + \mathcal{L}_{Var} + \mathcal{L}_{Mean}. \quad (9)$$

Correlation loss mainly focuses on the direction consistency between ground truth (GT) patches and predicted patches:

$$\mathcal{L}_{Corr} = \frac{1}{M} \sum_{i=0}^{M-1} 1 - \frac{\sum_{j=0}^{P-1} \left( y_j^{(i)} - \mu^{(i)} \right) \left( \hat{y}_j^{(i)} - \hat{\mu}^{(i)} \right)}{\sigma^{(i)} \hat{\sigma}^{(i)}} \quad (10)$$

where  $(\mu, \sigma)$  and  $(\hat{\mu}, \hat{\sigma})$  denote the mean and standard deviation of GT patches and predicted patches, respectively. M denotes the number of patches, and P represents the number of points within each patch. The variance loss quantifies the motion variability consistency between patches, ensuring that the predicted trajectory segments exhibit a similar range of motion deviations as the GT, which is essential for capturing the ego vehicle's acceleration/deceleration characteristics:

$$\mathcal{L}_{Var} = \frac{1}{M} \sum_{i=0}^{M-1} KL \left( \varphi \left( Y_p^{(i)} - \mu^{(i)} \right), \varphi \left( \hat{Y}_p^{(i)} - \hat{\mu}^{(i)} \right) \right) \quad (11)$$

where  $KL$  denotes the KL loss and  $\varphi$  denotes the SoftMax function. The mean loss measures the position deviation

between the centroid of predicted patches and GT patches, which constrains the overall spatial alignment of trajectory segments:

$$\mathcal{L}_{Mean} = \frac{1}{M} \sum_{i=0}^{M-1} |\mu_i - \hat{\mu}_i| \quad (12)$$

Our total training loss is:

$$\mathcal{L}_{total} = \alpha \mathcal{L}_{reg} + \beta \mathcal{L}_{cls} + \gamma \mathcal{L}_{patch} \quad (13)$$

where  $\alpha$ ,  $\beta$ , and  $\gamma$  are hyper parameters, respectively.

## IV. EXPERIMENTS

### A. Experiments Setup

**1) Datasets:** We evaluate the effectiveness of our proposed algorithm on two widely used large-scale public datasets. Argoverse is a motion forecasting dataset with diverse representative driving scenarios, derived from 1,006 hours of real-world driving data in Miami and Pittsburgh. For motion prediction, it leverages 2 seconds of observed trajectories of the target and neighboring agents to forecast the target's 3-second future trajectory. NuScenes focuses on complex urban lane scenarios in Boston and Singapore, covering a wide range of dynamic traffic environments. It contains over 1,000 20-second driving sequences, and its core prediction task is to generate five candidate trajectories for the target agent's 6-second future motion using 2 seconds of historical trajectory observations and surrounding context.

**2) Evaluation Metrics:** To assess alignment between multimodal predicted trajectories and ground truth (GT), we adopt four evaluation metrics: minimum Average Displacement Error ( $minADE_K$ ), minimum Final Displacement Error ( $minFDE_K$ ), rier minimum Final Displacement Error ( $b - minFDE_K$ ), and Miss Rate (MR). Specifically,  $minADE_K$  denotes the minimum mean L2 distance between the K predicted multimodal trajectories and GT across all time steps.  $minFDE_K$  focuses on the minimum L2 distance between endpoints of the K predicted trajectories and that of GT.  $b - minFDE_K$  is a variant of  $minFDE_K$ , with endpoint loss augmented by a  $(1.0 - \hat{p}_K)^2$  term. MR quantifies the proportion of predicted endpoints outside a 2-meter radius circle of GT endpoint.

### B. Quantitative Analysis

In this section, we quantitatively compare the performance of the proposed model against other state-of-the-art algorithms.

**1) Comparison with Map-free Methods:** The evaluation performance of our algorithm on the Nusences and Argoverse against other state-of-the-art algorithms is displayed in Table I. In these tables, \* indicates that map information is eliminated in the map-based methods.

On the NuScenes dataset, our method delivers competitive performance across all key evaluation metrics. Specifically, its  $minADE_5$  (1.34 m) outperforms representative map-free methods including MTR\* [10] and MLB [12]. For endpoint prediction accuracy, our  $minADE_5$  (2.89 m) also exhibits clear advantages over MLB and MTR\*. Our method achieves an identical  $minADE_{10}$  (1.13 m) to MTR\*, while its  $minFDE_{10}$

TABLE I  
EXPERIMENTAL RESULTS ON NUSCENES AND ARGOVERSE DATASETS  
(MAP-FREE)

NuScenes Dataset (Map-free)								
Method	Pub.	K=5			K=10			
		ADE	FDE	MR	ADE	FDE	MR	
Agentformer* [31]	ICCV 21'	1.97	4.21	/	1.58	3.14	/	
Map-free [32]	TIV 24'	1.70	3.67	0.65	1.30	2.58	0.52	
Laformer* [7]	CVPR 24'	1.57	/	/	1.32	/	/	
HeteGraph* [33]	ITSC 23'	/	/	/	1.31	2.43	0.60	
EA-Net [34]	ITS 24'	1.50	/	0.58	1.26	/	0.54	
MLB [12]	IoTJ 25'	1.48	3.13	0.52	1.18	2.27	0.36	
MTR* [10]	NeurIPS 22'	1.39	3.01	0.48	1.13	2.27	0.42	
Ours	/	1.34	2.89	0.51	1.13	2.28	0.39	

Argoverse Dataset (Map-free)					
Method	Pub.	$ADE_6$	$FDE_6$	$MR_6$	
mmTrans.* [8]	CVPR 21'	0.83	1.42	0.17	
STAM-P [15]	IoTJ 24'	0.82	1.30	0.15	
EBMP* [5]	ITS 23'	0.76	1.43	/	
Crat-Pred [23]	ICRA 22'	0.85	1.44	0.17	
HSTI [13]	ITS 25'	0.80	1.35	0.16	
HiVT64* [11]	CVPR 22'	0.77	1.25	0.14	
MLB [12]	IoTJ 25'	0.77	1.25	0.14	
Ours	/	0.75	1.18	0.12	

(2.28 m) is comparable to MLB and MTR\*. In terms of the MR metric, our  $MR_5$  (0.51) is slightly higher than MTR\* but superior to MLB, and our  $MR_{10}$  (0.39) outperforms MTR\* and is only marginally lower than the optimal result of MLB, significantly surpassing most other competing methods.

On the Argoverse dataset, our method maintains robust performance, attaining favorable  $minADE_6$  (0.75 m),  $minFDE_6$  (1.18 m), and  $MR_6$  (0.12) results. Notably, our method achieves comparative performance compared to state-of-the-art approaches such as HiVT64\* and MLB across both displacement error metrics and miss rate. These consistent improvements across two distinct benchmarks fully validate the effectiveness of the redundant information elimination mechanism integrated into our network.

2) *Comparison with Map-based Methods*: Map-based trajectory prediction models leverage precise map data to optimize predicted trajectories, as the embedded map information enables the model to gain deeper insights into vehicle behavioral patterns under complex traffic scenarios.

As shown in Table. II, on the NuScenes dataset, our map-free method achieves competitive performance against many map-based methods. Specifically, our  $minADE_5$  (1.34 m) matches DSCAM and outperforms mainstream map-based methods including Trajectron++, ContextVAE, and TGD. For  $minFDE_5$ , our result (2.89 m) is slightly higher than TGD but significantly superior to ContextVAE and other representative baselines. In terms of  $MR_5$ , our performance (0.51) is comparable to GC-GAT, and far better than early methods like Trajectron++ and G2LTraj. For  $MR_{10}$  (0.39), our performance is comparable with G2LTraj, only marginally lower than LAFormer (0.33) and much better than Trajectron++ (0.57), further verifying the robustness of our map-free approach.

On the Argoverse dataset, our method remains robust when compared to map-based counterparts. Our  $minADE_6$  (0.75 m)

TABLE II  
EXPERIMENTAL RESULTS ON NUSCENES AND ARGOVERSE DATASETS  
(MAP-BASED)

NuScenes Dataset (Map-based)								
Method	Pub.	K=5			K=10			
		ADE	FDE	MR	ADE	FDE	MR	
Trajectron++ [35]	ECCV 20'	1.88	/	0.70	1.51	/	0.57	
Autobot [36]	ICLR 22'	1.45	2.79	0.53	1.11	1.88	0.30	
G2LTraj [25]	arxiv 24'	1.40	/	0.63	0.96	/	0.39	
TGD [37]	TIV 24'	1.36	2.75	/	1.08	1.93	/	
DSCAM [26]	ITS 24'	1.34	/	0.45	/	/	/	
ContextVAE [17]	RAL 23'	1.59	3.28	/	/	/	/	
LAFormer [7]	CVPR 24'	1.19	/	0.48	0.93	/	0.33	
GC-GAT [24]	RAL 25'	1.19	/	0.52	1.06	/	0.49	
Ours	/	1.34	2.89	0.51	1.13	2.28	0.39	

Argoverse Dataset (Map-based)				
Method	Pub.	$ADE_6$	$FDE_6$	$MR_6$
HGO [38]	RAL 23'	0.78	1.45	/
I2T [39]	ITS 24'	0.76	1.20	0.12
MacFormer [9]	RAL 23'	0.71	1.05	0.10
HiVT [11]	CVPR 22'	0.66	0.96	0.10
LAFormer [7]	CVPR 24'	0.64	0.92	0.08
Ours	/	0.75	1.18	0.12

is higher than leading methods such as LAFormer and HiVT but outperforms HGO and I2T. For  $minFDE_6$ , our result (1.18 m) shows clear advantages over HGO and I2T, though lagging behind top-performing LAFormer and HiVT. Our  $MR_6$  (0.12) is on par with I2T and better than most baselines except LAFormer and HiVT. Overall, without relying on map information, our framework maintains a reasonable performance gap with advanced map-based methods and outperforms several mainstream baselines, fully validating its robustness and effectiveness.

### C. Comparison of Model Efficiency

To evaluate the practical applicability of our proposed model, we compare its inference efficiency and prediction accuracy with state-of-the-art trajectory prediction methods. As summarized in Table III, all methods are categorized into map-based and map-free approaches. The map-based method HiVT [11] requires 65 ms for inference. Among the map-free methods, our model achieves the comparative speed at 8 ms, which is 70 % faster than MLB [12] (27 ms). Meanwhile, CRAT-Pred [23] exhibits a significantly slower inference time of 178 ms. In terms of prediction accuracy, quantified by  $minFDE_6$ , our method achieves a value of 1.18, which is comparable to MLB and HiVT\* [11] (both 1.25) and outperforms HSTI (1.35) and CRAT-Pred (1.44). This demonstrates that our model achieves a favorable trade-off between inference efficiency and prediction accuracy, making it a competitive candidate for real-time trajectory prediction tasks such as autonomous driving.

### D. Ablation Study

In this chapter, we conduct an extensive ablation study to analyze the contribution of each component to the overall performance and the network's behavior under diverse scenarios.

TABLE III  
COMPARISON OF MODEL EFFICIENCY

Method	Categorization	Inference time (ms)	$minFDE_6$
HIVT [11]	map-based	65	0.96
HSTI [13]	map-free	10	1.35
HIVT* [11]	map-free	35	1.25
CRAT-Pred [23]	map-free	178	1.44
MLB [12]	map-free	27	1.25
our method	map-free	8	1.18

1) *Network components*: First, we ablate each key network component to evaluate its contribution to the overall prediction performance as shown in Table IV. Ablation results show that removing each component individually degrades key metrics, confirming their indispensable roles. Specifically, omitting the Frequency Filter retains low-frequency noise that contaminates agent interactions; lacking Temporal Trends deprives the model of local trend modeling, hindering fine-grained temporal dynamics capture; and the absence of TSAM/SSAM lacks selective attention, forcing the model to incorporate all temporal nodes or agents without distinction; and removing the Patch Loss weakens structural constraint on trajectory prediction, leading to outputs that further degrade prediction accuracy.

TABLE IV  
ABLATION STUDY ON CORE NETWORK COMPONENTS

ID	Frequency Filter	Temporal Trends	Patch			$ADE_5$	$FDE_5$	$MR_5$	$b - minFDE_5$
			TSAM	SSAM	Loss				
1	✓	✓	✓	✓	✓	1.34	2.89	0.51	3.47
2		✓	✓	✓	✓	1.37	2.93	0.52	3.50
3	✓		✓	✓	✓	1.37	2.94	0.51	3.50
4	✓	✓		✓	✓	1.35	2.94	0.53	3.50
5	✓	✓	✓		✓	1.36	2.96	0.52	3.52
6	✓	✓	✓	✓		1.36	2.96	0.52	3.52

Note: "✓" indicates the corresponding network component is enabled.

2) *Attention components*: Table V presents a comparative analysis of different attention mechanisms under the map-free trajectory prediction setting. ID 4 denotes Weighted Attention that simply weights and aggregates the two attentions. Our proposed Selective Attention outperforms Dense Attention, Sparse Attention, and Weighted Attention in key metrics ( $minADE$ ,  $minFDE$ ,  $MR$ ,  $b - minFDE$ ). By leveraging pair-wise relative information to achieve adaptive and efficient information selection, the proposed mechanism effectively balances the advantages of Dense Attention (comprehensive information coverage) and Sparse Attention (redundancy suppression), thereby yielding optimal trajectory prediction performance in complex interactive scenarios.

TABLE V  
COMPARISON OF MAP-FREE PREDICTION METHODS

ID	Dense attention	Sparse attention	$ADE_5$	$FDE_5$	$MR_5$	$b - FDE_5$
1	✓	✓	1.34	2.89	0.51	3.47
2	✓		1.41	3.02	0.53	3.57
3		✓	1.43	3.05	0.53	3.64
4	✓-	✓-	1.37	2.95	0.51	3.50

Note: "✓" indicates the attention component is enabled in the model.

### E. Qualitative Analysis

To provide intuitive insights into the effectiveness of our proposed algorithm, we visualize predicted trajectories across a diverse set of driving scenarios from the NuScenes validation dataset, encompassing straight driving, left-turn, and right-turn maneuvers. These scenarios are selected to reflect the complexity of real-world traffic, as they involve varying degrees of interaction with surrounding agents.

As depicted in Fig. 4, our model yields plausible multi-modal trajectory candidates for straight driving, left-turn, and right-turn scenarios, with straight driving achieving distinctly superior prediction performance. Straight trajectories demonstrate tighter alignment with ground truth, attributed to their stable linear motion and consistent velocity—traits that render historical motion patterns highly predictable, while our cross-domain redundancy elimination mechanism efficiently filters out extraneous noise and select important features. In contrast, turning maneuvers entail non-linear motion dynamics and intricate interactions with surrounding agents. Without HD map guidance to inform directional constraints and traffic rules, these inherent complexities result in relatively larger prediction deviations. Nevertheless, our model still delivers reliable trajectory estimates even in turning scenarios, underscoring its effectiveness in both stable, low-interaction contexts and more complex driving environments.

## V. CONCLUSION

In summary, this study proposes a map-free trajectory prediction algorithm for complex interactive autonomous driving scenarios, integrating temporal, spatial, and frequency domain information via a MoE mechanism, selective attention module, and multimodal decoder with additional patch-level loss supervision. Experimental results on NuScenes and Argoverse datasets validate that the algorithm effectively filters redundant data, strengthens cross-domain feature fusion and representation, enhances computational efficiency and prediction accuracy, and provides a reliable solution for handling intricate agent interactions in real-world autonomous driving systems.

## REFERENCES

- [1] J. Gao, C. Sun, H. Zhao, Y. Shen, D. Anguelov, C. Li, and C. Schmid, “VectorNet: Encoding hd maps and agent dynamics from vectorized representation,” in *Proceedings of the IEEE/CVF conference on Computer Vision and Pattern Recognition*, 2020, pp. 11 525–11 533.
- [2] M. Liang, B. Yang, R. Hu, Y. Chen, R. Liao, S. Feng, and R. Urtasun, “Learning lane graph representations for motion forecasting,” in *European Conference on Computer Vision*, 2020, pp. 541–556.
- [3] X. Jia, P. Wu, L. Chen, Y. Liu, H. Li, and J. Yan, “HDGT: Heterogeneous driving graph transformer for multi-agent trajectory prediction via scene encoding,” *IEEE transactions on pattern analysis and machine intelligence*, vol. 45, no. 11, pp. 13 860–13 875, 2023.
- [4] W. Xiong, J. Chen, and Z. Qi, “Fine-grained behavior and lane constraints guided trajectory prediction method,” *arXiv preprint arXiv:2503.21477*, 2025.
- [5] C. Gómez-Huélamo, M. V. Conde, R. Barea, M. Ocaña, and L. M. Bergasa, “Efficient baselines for motion prediction in autonomous driving,” *IEEE Transactions on Intelligent Transportation Systems*, vol. 25, no. 5, pp. 4192–4205, 2023.
- [6] G. Xin, D. Chu, L. Lu, Z. Deng, Y. Lu, and X. Wu, “Multi-agent trajectory prediction with difficulty-guided feature enhancement network,” *IEEE Robotics and Automation Letters*, 2025.

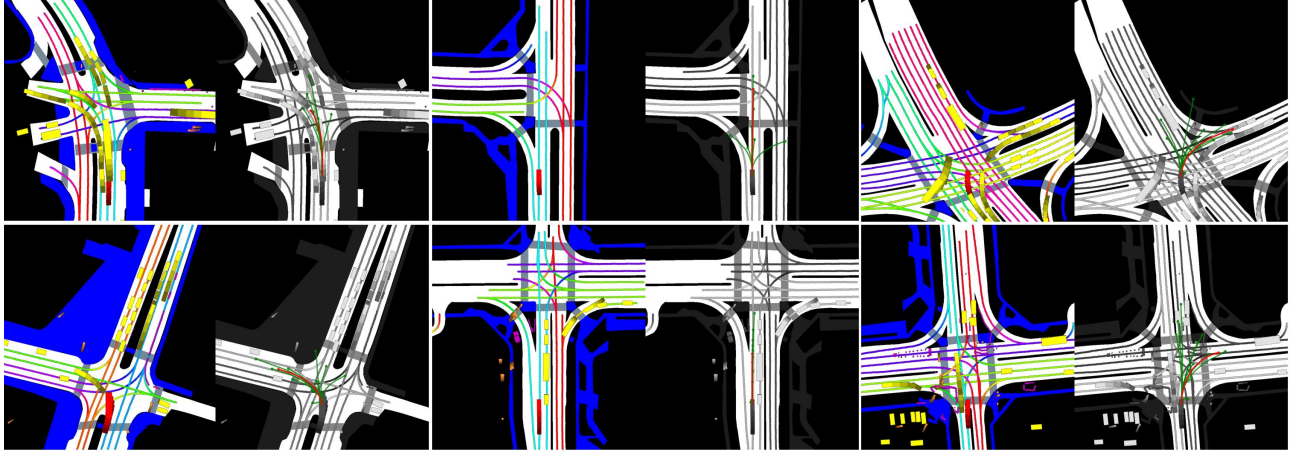


Fig. 4. Visualization of Predicted Trajectories Using Our Proposed Algorithm on Diverse Traffic Scenarios. Red trajectories stand for the ground truth, green multi-modal trajectories represent our predicted results, and yellow blocks denote the surrounding vehicle historical trajectories.

- [7] M. Liu, H. Cheng, L. Chen, H. Broszio, J. Li, R. Zhao, M. Sester, and M. Y. Yang, “Laformer: Trajectory prediction for autonomous driving with lane-aware scene constraints,” in *Proceedings of the IEEE/CVF conference on Computer Vision and Pattern Recognition*, 2024, pp. 2039–2049.
- [8] Y. Liu, J. Zhang, L. Fang, Q. Jiang, and B. Zhou, “Multimodal motion prediction with stacked transformers,” in *Proceedings of the IEEE/CVF conference on Computer Vision and Pattern Recognition*, 2021, pp. 7577–7586.
- [9] C. Feng, H. Zhou, H. Lin, Z. Zhang, Z. Xu, C. Zhang, B. Zhou, and S. Shen, “Macformer: Map-agent coupled transformer for real-time and robust trajectory prediction,” *IEEE Robotics and Automation Letters*, vol. 8, no. 10, pp. 6795–6802, 2023.
- [10] S. Shi, L. Jiang, D. Dai, and B. Schiele, “Motion transformer with global intention localization and local movement refinement,” *Advances in Neural Information Processing Systems*, vol. 35, pp. 6531–6543, 2022.
- [11] Z. Zhou, L. Ye, J. Wang, K. Wu, and K. Lu, “HiVT: Hierarchical vector transformer for multi-agent motion prediction,” in *Proceedings of the IEEE/CVF conference on Computer Vision and Pattern Recognition*, 2022, pp. 8823–8833.
- [12] Y. Ren, L. Liu, Z. Lan, Z. Cui, and H. Yu, “Mlb-traj: Map-free trajectory prediction with local behavior query for autonomous driving,” *IEEE Internet of Things Journal*, 2025.
- [13] X. Luo, S. Fu, B. Gao, Y. Zhao, H. Tan, and Z. Song, “Hsti: A light hierarchical spatial-temporal interaction model for map-free trajectory prediction,” *IEEE Transactions on Intelligent Transportation Systems*, 2025.
- [14] N. Shazeer, A. Mirhoseini, K. Maziarz, A. Davis, Q. Le, G. Hinton, and J. Dean, “Outrageously large neural networks: The sparsely-gated mixture-of-experts layer,” *arXiv preprint arXiv:1701.06538*, 2017.
- [15] Y. Hou, X. Zhang, H. Zhang, X. Cao, Z. Lu, and X. Yuan, “A vehicle trajectory prediction model for map-free scenes using the spatiotemporal attentional mechanism,” *IEEE Internet of Things Journal*, vol. 12, no. 9, pp. 11 372–11 382, 2024.
- [16] J. Chung, C. Gulcehre, K. Cho, and Y. Bengio, “Empirical evaluation of gated recurrent neural networks on sequence modeling. arxiv 2014,” *arXiv preprint arXiv:1412.3555*, vol. 1412, 2014.
- [17] P. Xu, J.-B. Hayet, and I. Karamouzas, “Context-aware timewise vae’s for real-time vehicle trajectory prediction,” *IEEE Robotics and Automation Letters*, vol. 8, no. 9, pp. 5440–5447, 2023.
- [18] S. Hochreiter and J. Schmidhuber, “Long short-term memory,” *Neural computation*, vol. 9, no. 8, pp. 1735–1780, 1997.
- [19] A. Gu and T. Dao, “Mamba: Linear-time sequence modeling with selective state spaces,” in *First conference on language modeling*, 2024.
- [20] A. Vaswani, N. Shazeer, N. Parmar, J. Uszkoreit, L. Jones, A. N. Gomez, Ł. Kaiser, and I. Polosukhin, “Attention is all you need,” *Advances in neural information processing systems*, vol. 30, 2017.
- [21] Z. Zhang, D. Guo, S. Zhou, J. Zhang, and Y. Lin, “Flight trajectory prediction enabled by time-frequency wavelet transform,” *Nature Communications*, vol. 14, no. 1, p. 5258, 2023.
- [22] X. Chen, L. Zeng, M. Gao, C. Ding, and Y. Bian, “Diffwt: Diffusion-based pedestrian trajectory prediction with time-frequency wavelet transform,” *IEEE Internet of Things Journal*, 2024.
- [23] J. Schmidt, J. Jordan, F. Gritschneider, and K. Dietmayer, “Crat-pred: Vehicle trajectory prediction with crystal graph convolutional neural networks and multi-head self-attention,” in *2022 International Conference on Robotics and Automation*, 2022, pp. 7799–7805.
- [24] M. Gulzar, Y. Muhammad, and N. Muhammad, “Gc-gat: Multimodal vehicular trajectory prediction using graph goal conditioning and cross-context attention,” *IEEE Robotics and Automation Letters*, 2025.
- [25] Z. Zhang, Z. Hua, M. Chen, W. Lu, B. Lin, D. Cai, and W. Wang, “G2ltraj: A global-to-local generation approach for trajectory prediction,” *arXiv preprint arXiv:2404.19330*, 2024.
- [26] L. Li, X. Wang, J. Lian, J. Zhao, and J. Hu, “Efficient vehicle trajectory prediction with goal lane segments and dual-stream cross attention,” *IEEE Transactions on Intelligent Transportation Systems*, 2024.
- [27] Z. Liu, “Freqmoe: Enhancing time series forecasting through frequency decomposition mixture of experts,” *arXiv preprint arXiv:2501.15125*, 2025.
- [28] Y. Nie, “A time series is worth 64words: Long-term forecasting with transformers,” *arXiv preprint arXiv:2211.14730*, 2022.
- [29] S. Zhou, D. Chen, J. Pan, J. Shi, and J. Yang, “Adapt or perish: Adaptive sparse transformer with attentive feature refinement for image restoration,” in *Proceedings of the IEEE/CVF conference on Computer Vision and Pattern Recognition*, 2024, pp. 2952–2963.
- [30] D. Kudrat, Z. Xie, Y. Sun, T. Jia, and Q. Hu, “Patch-wise structural loss for time series forecasting,” *arXiv preprint arXiv:2503.00877*, 2025.
- [31] Y. Yuan, X. Weng, Y. Ou, and K. M. Kitani, “Agentformer: Agent-aware transformers for socio-temporal multi-agent forecasting,” in *Proceedings of the IEEE/CVF International Conference on Computer Vision*, 2021, pp. 9813–9823.
- [32] J. Xiang, Z. Nan, Z. Song, J. Huang, and L. Li, “Map-free trajectory prediction in traffic with multi-level spatial-temporal modeling,” *IEEE Transactions on Intelligent Vehicles*, vol. 9, no. 2, pp. 3258–3270, 2023.
- [33] D. Grimm, M. Zipf, F. Hertlein, A. Naumann, J. Luettin, S. Thoma, S. Schmid, L. Halilaj, A. Rettinger, and J. M. Zöllner, “Heterogeneous graph-based trajectory prediction using local map context and social interactions,” in *2023 IEEE 26th international conference on intelligent transportation systems (ITSC)*, 2023, pp. 2901–2907.
- [34] J. Chen, Z. Wang, J. Wang, and B. Cai, “Q-eanet: Implicit social modeling for trajectory prediction via experience-anchored queries,” *IET Intelligent Transport Systems*, vol. 18, no. 6, pp. 1004–1015, 2024.
- [35] T. Salzmann, B. Ivanovic, P. Chakravarty, and M. Pavone, “Trajectron++: Dynamically-feasible trajectory forecasting with heterogeneous data,” in *European Conference on Computer Vision*, 2020, pp. 683–700.
- [36] R. Girgis, F. Golemo, F. Codevilla, M. Weiss, J. A. D’Souza, S. E. Khou, F. Heide, and C. Pal, “Latent variable sequential set transformers for joint multi-agent motion prediction,” *arXiv preprint arXiv:2104.00563*, 2021.
- [37] J. Wang, J. Guo, M. Feng, C. Li, X. Xue, and J. Pu, “Trajectory grid diffusion for multimodal trajectory prediction in autonomous vehicles,” *IEEE Transactions on Intelligent Vehicles*, 2024.

- [38] X. Mo, Y. Xing, H. Liu, and C. Lv, "Map-adaptive multimodal trajectory prediction using hierarchical graph neural networks," *IEEE Robotics and Automation Letters*, vol. 8, no. 6, pp. 3685–3692, 2023.
- [39] Y. Zhou, Z. Wang, N. Ning, Z. Jin, N. Lu, and X. Shen, "I2t: from intention decoupling to vehicular trajectory prediction based on priorformer networks," *IEEE Transactions on Intelligent Transportation Systems*, vol. 25, no. 8, pp. 9411–9426, 2024.